First-principles study of the structural phase transformation of hafnia under pressure

Joongoo Kang, E.-C. Lee, and K. J. Chang
Department of Physics, Korea Advanced Institute of Science and Technology, Daejeon 305-701, Korea
(Received 18 February 2003; revised manuscript received 22 May 2003; published 7 August 2003)

We investigate the phase transformation of HfO_2 under hydrostatic pressure through first-principles pseudopotential calculations within the local-density-functional approximation (LDA) and the generalized gradient approximation (GGA). We find that with increasing of pressure, HfO_2 undergoes a series of structural transformations from monoclinic to orthorhombic I and then to orthorhombic II, consistent with experiments. The calculated transition pressures within the GGA are in good agreement with the measured values, while they are severely underestimated by the LDA. Analyzing the distribution of electron densities for the high-pressure phases, we find that the electron densities of the orthorhombic-II phase are more homogeneous than for the orthorhombic-I phase. Due to this distinct difference in the homogeneity of electron densities, the energy difference between the orthorhombic-I and orthorhombic-II phases is enhanced in the GGA; thus, the transition pressure between the two phases increases significantly.

DOI: 10.1103/PhysRevB.68.054106 PACS number(s): 61.50.Ks, 64.60.−i, 71.15.Nc, 71.20.−b

I. INTRODUCTION

Hafnia (HfO_2) is a wide-band-gap material with a high dielectric constant, and this material has recently received much attention because of its potential application for alternative dielectrics to SiO_2 in microelectronic devices. Several experiments have demonstrated that thin HfO_2 films deposited on Si lead to low leakage current and high thermal stability.[1,2] As for other applications, HfO_2 is considered to be a good candidate for hard materials, because the orthorhombic-II (cotunnite) structure, which is one of the high-pressure phases of HfO_2, has a very large bulk modulus of 312 GPa.[3]

At ambient conditions, HfO_2 has a monoclinic baddeleyite structure with the space group $P2_1/c$ and sequentially transforms into the orthorhombic-I (*Pbca*) and then into the orthorhombic-II (*Pnma*) phase as pressure increases. In *in situ* x-ray diffraction measurements under high pressure and high temperature,[3] the orthorhombic-I phase is found to be stable for pressures between 4 and 14.5 GPa below 1250–1400°C, while the orthorhombic-II phase appears above 14.5 GPa and is stable up to 1800°C at 21 GPa. High-pressure Raman spectroscopy studies[4] at room temperature reported similar results with the transition pressures of 4.3 and 12 GPa for the orthorhombic-I and orthorhombic-II phases, respectively, while other experiments[5,6] showed much higher transition pressures of 10 and 30 GPa.

In very recent theoretical calculations based on the generalized gradient approximation (GGA),[7,8] although the monoclinic, cubic, and tetragonal structures were considered, main interests were the dielectric constant and the defect properties of O-related defects. Other theoretical work using the local-density-functional approximation (LDA) was reported for the structural phase transformation of HfO_2 under pressure.[9] However, the pressure-induced structural sequence was shown to be inconsistent with experiments; the monoclinic phase is directly transformed into the orthorhombic-II phase, while the orthorhombic-I phase is energetically unfavorable. In the LDA calculations, the cohesive energies of materials are generally overestimated, and the transition pressures in pressure-induced structural transformations are underestimated.[10,11] The use of the GGA has been very successful in remedying the failure of the LDA.

In this paper, we investigate the structural phase transformation of HfO_2 under hydrostatic pressure through first-principles pseudopotential calculations. Both the LDA and GGA calculations show that HfO_2 undergoes a series of structural transformations from monoclinic to orthorhombic I and then to orthorhombic II, with increasing of pressure, consistent with experiments. By including the GGA correction for the exchange-correlation potential, we find that the calculated pressures for the monoclinic–to–orthorhombic-I and orthorhombic-I–to–orthorhombic-II transitions are in better agreement with the measured values. To analyze the improvement of the transition pressure by the GGA, we examine the distribution of electron charge densities for the high-pressure phases and also investigate the electronic structure of HfO_2.

II. COMPUTATIONAL METHOD

Our calculations are based on the first-principles pseudopotential method within the local-density-functional approximation. Norm-conserving nonlocal pseudopotentials are generated by the scheme of Troullier and Martins[12] and transformed into a separable form of Kleinman and Bylander.[13] For the Hf atom, we include a nonlinear partial core correction[14] for the exchange-correlation functional to deal with the overlap between the core and valence electron densities. For the LDA exchange-correlation functional, we use the Ceperley-Alder expression as parametrized by Perdew and Zunger.[15] We also perform GGA calculations, with use of the functional form suggested by Perdew, Burke, and Ernzerhof.[16] We consider various phases such as monoclinic, cubic, tetragonal, $Pbc21$, and orthorhombic (I and II) structures for studying pressure-induced structural phase transformations. The wave functions are expanded in a plane-wave basis set with a kinetic energy cutoff of 60 Ry throughout this work, with which the total energies (E_{tot}) are converged to within 1 mRy per atom. Testing a higher energy cutoff of

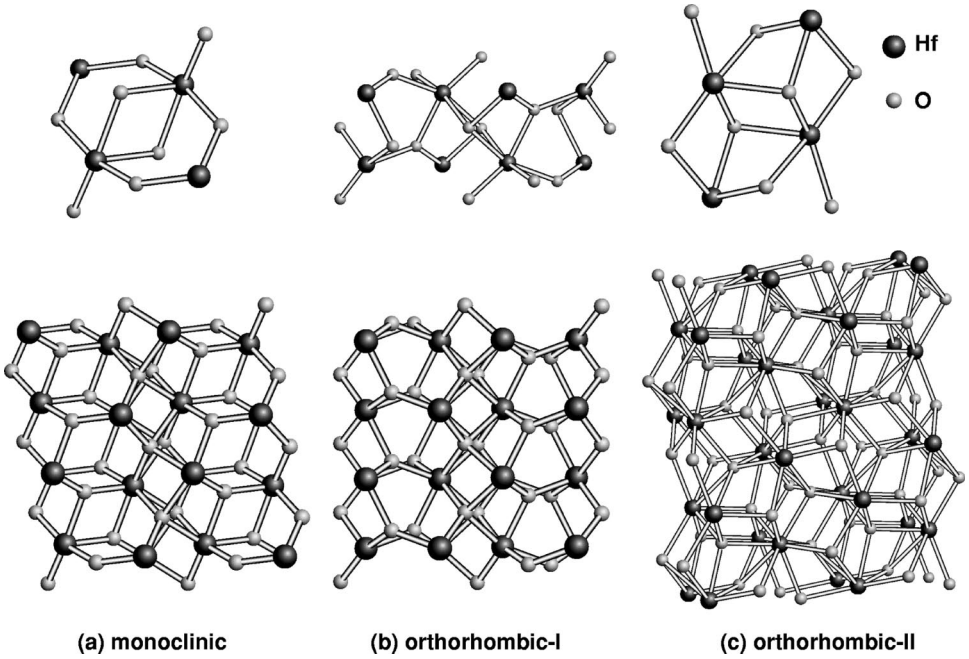

FIG. 1. The ball-and-stick models for the primitive unit cells (up) and their expanded crystal structures (bottom) of the (a) monoclinic, (b) orthorhombic-I, and (c) orthorhombic-II structures of HfO_2.

100 Ry, we find that the change of the total energy difference between the monoclinic and orthorhombic-I phases is less than 0.01 mRy per atom, so that transition pressures are well converged with the kinetic energy cutoff of 60 Ry. The Brillouin-zone summation of the charge densities is performed using a uniform grid of **k** points, choosing 10, 4, and 12 **k** points in the irreducible sectors for the monoclinic, orthorhombic-I, and orthorhombic-II structures, respectively, and the total energies are found to have errors within 0.1 mRy per atom. For each phase, we calculate the total energies for many different cell volumes. For a fixed volume, we optimize all the lattice parameters and relax internal parameters using the conjugate gradient method.

III. RESULTS AND DISCUSSIONS

First we discuss the details of various structures considered here. The ball-and-stick models for the monoclinic, orthorhombic-I, and orthorhombic-II structures are shown in Fig. 1. In the monoclinic structure, there are two types of O atoms, which are threefold and fourfold coordinated, while all the Hf atoms are in a sevenfold-coordinated configuration. A threefold-coordinated O and its three neighboring Hf atoms lie in a nearly flat plane. The monoclinic structure has 4 formula units of HfO_2 per primitive cell. In the orthorhombic-I phase, which first appears as a high-pressure phase, the size of the primitive cell is doubled, while the coordination numbers of Hf and O remain unchanged. On the other hand, the orthorhombic-II phase, which is stabilized for further increase of pressure, has higher coordination numbers, with the same units of HfO_2 in the primitive cell as the monoclinic phase; the coordination number of Hf increases from 7 to 9, and the O atom is either fourfold or fivefold coordinated. In addition to the monoclinic, orthorhombic-I, and orthorhombic-II phases, we also consider the tetragonal ($P4_2/nmc$), cubic ($Fm3m$), and $Pbc21$ phases. The tetragonal and cubic phases are stable at high temperatures under atmospheric pressure. The monoclinic phase at low temperature was shown to transform into a tetragonal structure above 2000 K and then into a cubic structure above 2870 K. Previous LDA calculations[9] showed

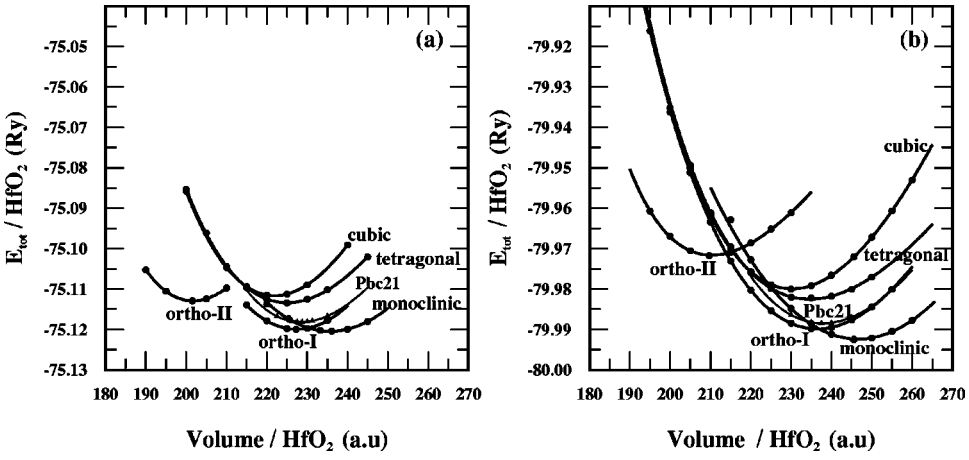

FIG. 2. The total energies (per HfO_2 formula) vs volume in the (a) LDA and (b) GGA calculations.

TABLE I. Calculated structural parameters for the monoclinic, cubic, and tetragonal phases of HfO_2 in the GGA and LDA. Here V_0 (in units of Å^3) and B_0 (in GPa) denote the equilibrium volume per HfO_2 formula and the bulk modulus, respectively, the lattice parameters (in Å) are given by a, b, and c, and β (in degree) is the angle between the lattice parameters. The internal coordinates of the Hf and O atoms are given by x, y, and z, and δz in the tetragonal phase is the shift of the O atom in fractional coordinates with respect to the ideal cubic position.

	Present GGA	Previous GGA [a]	Present LDA	Previous LDA [b]	Expt. [c]
Monoclinic					
V_0	36.39	34.81	34.98	34.55	34.62
a	5.215	5.132	5.135	5.12	5.119
b	5.293	5.189	5.244	5.17	5.170
c	5.350	5.307	5.269	5.29	5.298
β	99.73	99.78	99.54	99.25	99.18
B_0	192		186	251	185
Hf(x)	0.277	0.277	0.279	0.279	0.276
Hf(y)	0.042	0.044	0.042	0.042	0.040
Hf(z)	0.207	0.209	0.208	0.211	0.207
O1(x)	0.076	0.070	0.078	0.072	0.071
O1(y)	0.343	0.333	0.350	0.340	0.332
O1(z)	0.335	0.345	0.331	0.343	0.344
O2(x)	0.447	0.448	0.445	0.449	0.446
O2(y)	0.759	0.758	0.760	0.758	0.755
O2(z)	0.483	0.478	0.485	0.481	0.480
Cubic					
V_0	34.10	32.49	32.89	33.95	32.77
a	5.148	5.07	5.086	5.14	5.08
B_0	257		289	280	
Tetragonal					
V_0	34.82	33.12	33.34		35.075
a	5.17	5.06	5.09		5.15
c	5.22	5.181	5.14		5.289
δz	0.033	0.051	0.033		
B_0	183		228		

[a]Reference 8.
[b]Reference 9.
[c]References 18–20.

TABLE II. Calculated structural parameters for the orthorhombic-I and orthorhombic-II phases of HfO_2 in the GGA and LDA. Here V_0 (in units of Å^3) and B_0 (in GPa) denote the equilibrium volume per HfO_2 formula and the bulk modulus, respectively, and the lattice parameters (in Å) are given by a, b, and c. The internal coordinates of the Hf and O atoms are given by x, y, and z.

	Present GGA	Present LDA	Previous LDA [a]	Expt. [b]
Orthorhombic I				
V_0	35.04	33.67	34.46	
a	10.215	10.079	10.22	
b	5.324	5.266	5.31	
c	5.154	5.075	5.08	
B_0	221	251	256	220
Hf(x)	0.885	0.885	0.884	
Hf(y)	0.036	0.035	0.033	
Hf(z)	0.256	0.255	0.255	
O1(x)	0.791	0.791	0.791	
O1(y)	0.375	0.376	0.371	
O1(z)	0.127	0.128	0.131	
O2(x)	0.977	0.977	0.977	
O2(y)	0.738	0.738	0.747	
O2(z)	0.497	0.497	0.494	
Orthorhombic II				
V_0	31.18	29.89	30.66	
a	5.629	5.557	5.48	
b	3.353	3.293	3.35	
c	6.606	6.531	6.68	
B_0	252	295	306	312
Hf(x)	0.247	0.245	0.249	
Hf(y)	0.250	0.250	0.250	
Hf(z)	0.113	0.115	0.115	
O1(x)	0.360	0.359	0.360	
O1(y)	0.250	0.250	0.250	
O1(z)	0.426	0.426	0.425	
O2(x)	0.022	0.025	0.022	
O2(y)	0.750	0.750	0.750	
O2(z)	0.339	0.337	0.339	

[a]Reference 9.
[b]Reference 3.

that the $Pbc21$ phase has an equilibrium volume similar to that of the orthorhombic-I phase but a lower total energy. The primitive cells of the cubic, tetragonal, and $Pbc21$ structures contain 1, 2, and 4 formula units of HfO_2, respectively. For each volume, we optimize the c/a ratio for the tetragonal phase, three lattice parameters for the monoclinic structure, and two parameters for the orthorhombic-I, orthorhombic-II, and $Pbc21$ structures.

The calculated total energies in the LDA and GGA are plotted as a function of volume and compared with each other in Fig. 2. The total energies are then fitted to the Murnaghan equation of state[17] to obtain the equilibrium volume V_0, the bulk modulus B_0, and the ground-state energy E_0. Our results for the lattice parameters (a, b, and c), internal parameters for the Hf and O atoms, V_0, and B_0 are listed for all the phases considered here and compared with experiments and other calculations in Tables I and II.

For the monoclinic phase, we find that the LDA results for V_0 and B_0 are in slightly better agreement with experiments with errors of about 1%, compared with the GGA results. In the GGA, the equilibrium volume is larger by about 5%, which is the usual tendency of slightly increasing interatomic distances, and the bulk modulus is increased by about 4%. The LDA result of $B_0=186$ GPa is very close to one experimentally measured value of 185 GPa,[4] while the other experimental value is 284 GPa.[5] For the internal coordinates of Hf and O, both the LDA and GGA give similar results, in

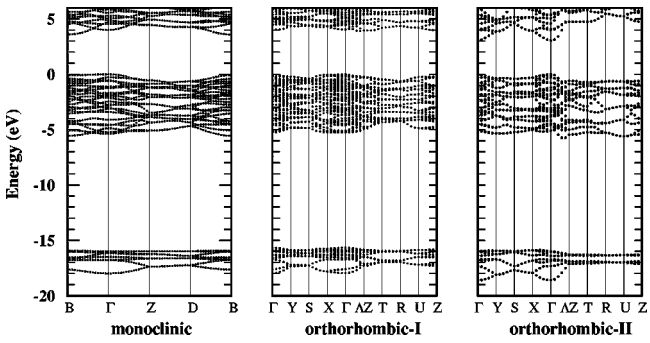

FIG. 3. The band structures for the monoclinic, orthorhombic-I, and orthorhombic-II phases at their equilibrium volumes of HfO_2.

good agreement with experiments. For the cubic phase, we also find that the LDA result for V_0 is in better agreement with the measured value, while the GGA value is larger by about 4%. For the tetragonal phase, however, the GGA values for V_0, a, and c are closer to the measured values, as compared to the LDA results. For the orhorhombic-I and orhorhombic-II phases, the GGA equilibrium volumes are also found to increase by about 4%, compared with the LDA results. Among the phases considered, the orthorhombic-II phase has the largest bulk modulus of 312 GPa,[3] suggesting a good candidate for hard materials. Similar to other phases, the bulk moduli for both the orhorhombic-I and orhorhombic-II phases are reduced with the GGA correction. The GGA value of $B_0=221$ GPa in the orhorhombic-I phase is in good agreement with the measured value of 220 GPa, while it is lower by about 19% for the orhorhombic-II phase.

Previous theoretical calculations are listed and compared with our results in Tables I and II. For the monoclinic phase, the overall results of Lowther and co-workers[9] using the LDA are comparable to our LDA calculations, while their calculated bulk modulus of 251 GPa is much larger than our result of 186 GPa. The large difference in the bulk modulus between the two calculations may result from the fact that they fix the angle β between the lattice vectors, while β is optimized for each volume in our calculations. There have been two theoretical calculations using the GGA for the monoclinic and cubic phases. The previous GGA results[8] for V_0 and the lattice parameters, which were obtained using the ultrasoft pseudopotentials[21] within the GGA of Perdew,[22] are in slightly better agreement with experiments than our GGA results employing the norm-conserving pseudopotentials. However, other GGA calculations[7] using the ultrasoft pseudopotentials showed larger deviations from the experimental results. For the $Pbc21$ phase, our LDA results for V_0 and B_0 are 33.9 Å^3 per formula unit and 250 GPa, respectively, as compared to other LDA calculations of $V_0=34.5$ Å^3 and $B_0=272$ GPa.[9]

The band structures for various phases of HfO_2 are drawn in Fig. 3. In the GGA calculations, HfO_2 is found to have indirect band gaps of 3.6 and 3.9 eV for the monoclinic and orthorhombic-I phases, respectively, whereas the orthorhombic-II phase has a direct gap of 3.1 eV. For all the phases, the LDA band gaps are generally smaller by about 0.1 eV than the GGA results. For the monoclinic phase, the

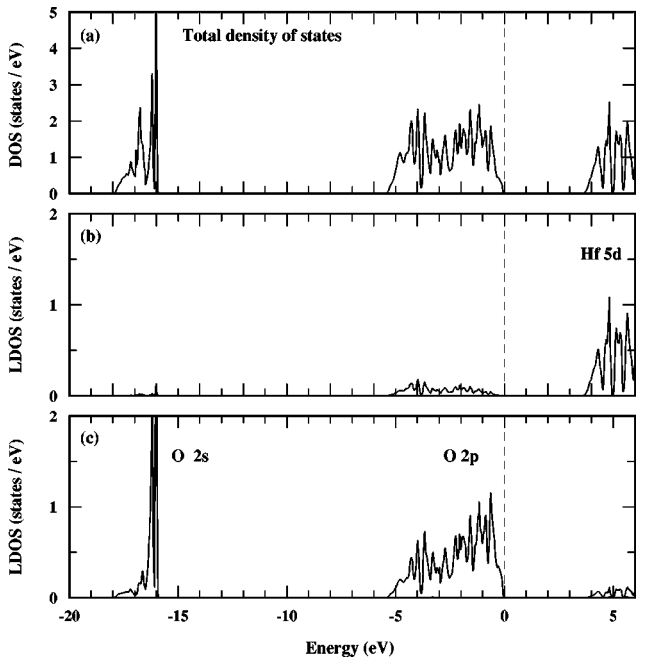

FIG. 4. (a) The total density of states and local densities of states projected onto the (b) Hf and (c) O atoms in the monoclinic structure.

calculated band gap is underestimated by about 37%, as compared to the experimentally measured value of 5.68 eV.[23] Figure 4 shows the density of states (DOS) and the local density of states (LDOS) projected onto the Hf and O atoms at the equilibrium volume of the monoclinic phase. We find that the O $2s$ and $2p$ bands are centered at around -17 and -3 eV, respectively, below the valence-band edge, while the Hf $5d$ band lies in the conduction band, indicating that Hf valence electrons are almost completely transferred to the surrounding O atoms. Thus, the valence electrons are mostly localized around the O atoms, with weak directional bonds to the Hf atoms, as shown in Fig. 5.

A transition pressure (P_t) between two phases can be estimated by the crossing point of their enthalpies which are equivalent to the Gibbs free energy at zero temperature. The enthalpy differences with respect to the monoclinic phase are drawn as a function of pressure in Fig. 6(a). Recent *in situ* x-ray measurements[3] showed that the monoclinic phase first transforms into the orthorhombic-I phase at a pressure of 4 GPa and then successively into the orthorhombic-II phase at 14.5 GPa. A similar transition sequence was observed by high-pressure Raman spectroscopy studies,[4] which reported transition pressures of 4.3 and 12 GPa. In our calculations, we also find a transition sequence from monoclinic to orthorhombic I and then to orthorhombic II, in good agreement with experiments. However, the $Pbc21$ phase is found to be unstable against the orthorhombic-I structure, while other LDA calculations[9] showed that a direct transition occurs from monoclinic to orthorhombic II, and the $Pbc21$ phase is lower in energy than the orthorhombic-I phase. The calculated transition pressures are listed in Table III. For the transition from monoclinic to orthorhombic I, the GGA transition pressure is estimated to be 3.8 GPa, in good agreement with

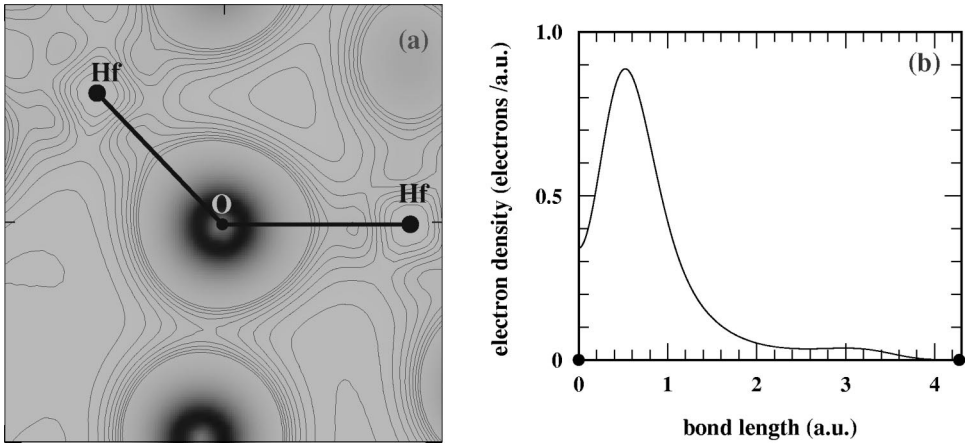

FIG. 5. (a) The contour plot of electron charge densities and (b) the line charge densities along the O-Hf bond in the monoclinic phase.

experiments, while the LDA value of 0.9 GPa is severely underestimated. Similarly, for the transition from orthorhombic I to orthorhombic II, we find a significant improvement of the transition pressure from 4.1 to 10.6 GPa with the GGA correction. In this case, the GGA value for P_t is still lower by 11%–27% than the measured values, and this large error may result from the underestimation of the bulk modulus for the orthorhombic-II phase. From the equation of state [see Fig. 6(b)], we estimate the transition volumes for each transition. Compared with the LDA values, the GGA calculations give better agreements of the transition volumes with experiments, as shown in Table III. In the GGA calculations, the volume change occurs from $0.980V_0^{mono}$ to $0.943V_0^{mono}$ for the monoclinic–to–orthorhombic-I transition, while the measured values are $0.97V_0^{mono}$ and $0.94V_0^{mono}$, where V_0^{mono} is the equilibrium volume of the monoclinic phase. For the orthorhombic-I–to-orthorhombic-II transition, the transition volumes are calculated to be $0.917V_0^{mono}$ and $0.820V_0^{mono}$, close to the measured values of $0.90V_0^{mono}$ and $0.82V_0^{mono}$.

Since the transition pressure is obtained by the slope of the common tangent line between the total energy curves, it sensitively depends on the total energy difference (ΔE_0) between two phases at their equilibrium volumes (V_0). The LDA and GGA results for V_0 and ΔE_0 relative to the monoclinic phase are summarized in Table IV. For the phases considered here, the GGA generally increases ΔE_0 and V_0, compared with the LDA results. In this case, the increase of V_0, which is defined as $[V_0(\mathrm{GGA})-V_0(\mathrm{LDA})]/V_0(\mathrm{LDA})$, is found to be about 4%, almost the same for each phase, while the increase of ΔE_0 by the GGA is largest for the orthorhombic-II phase. Since the total energies of both the orthorhombic-I and orthorhombic-II phases relative to the monoclinic phase increase, the transition pressures are greatly enhanced by the GGA, especially for the orthorhombic-I–to–orthorhombic-II transition. It is interesting to note that the increase of ΔE_0 by the GGA depends on the equilibrium volume of each structure. In Fig. 7, $[\Delta E_0(\mathrm{GGA})-\Delta E_0(\mathrm{LDA})]$ is plotted as a function of the normalized equilibrium volume, $V_0(\mathrm{LDA})/V_0^{mono}(\mathrm{LDA})$, and the increase of ΔE_0 for the compressed phase becomes more significant as the volume decreases.

To see the effect of the GGA correction on ΔE_0, we examine the distribution of electron densities for different phases. In Fig. 8, the volume of the part of the Wigner-Seitz cell having a density parameter r_s within the interval r_s and $r_s+\Delta r_s$, divided by the equilibrium volume times Δr_s,[10] is plotted as a function of r_s, where r_s is defined by $r_s=(3/4\pi n)^{1/3}$, with n denoting the particle density. Similarly, the volume of the part of the Wigner-Seitz cell having a density gradient parameter s within the interval s and $s+\Delta s$, normalized by the equilibrium volume times Δs, is

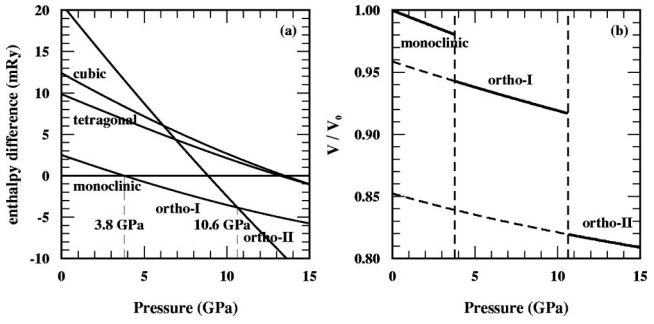

FIG. 6. (a) The enthalpies of various phases with respect to that of the monoclinic phase and (b) the equations of states are plotted in the GGA calculations.

TABLE III. Transition pressures and volume changes in the pressure-induced structural phase transformations of HfO_2. Here P_t (in GPa) and V_t (in V_0^{mono}) denote the transition pressure and transition volume, respectively, where V_0^{mono} is the equilibrium volume of the monoclinic phase.

	LDA	GGA	Expt.
Monoclinic → orthorhombic I			
P_t	0.9	3.8	4, [a] 4.3 [b]
V_t^{mono}	0.995	0.980	0.97 [a]
$V_t^{ortho\text{-}I}$	0.961	0.943	0.94 [a]
Orthorhombic I → orthorhombic II			
P_t	4.1	10.6	14.5, [a] 12 [b]
$V_t^{ortho\text{-}I}$	0.949	0.917	0.90 [a]
$V_t^{ortho\text{-}II}$	0.844	0.820	0.82 [a]

[a]Reference 3.
[b]Reference 4.

TABLE IV. The equilibrium volumes (V_0 in units of Å^3 per HfO_2 formula) and the ground-state energy differences (ΔE_0 in units of meV) of various phases relative to the monoclinic phase in the LDA and GGA calculations are listed. Here ΔV_0 is given by $\Delta V_0 = V_0(\mathrm{GGA}) - V_0(\mathrm{LDA})$.

	Monoclinic	Ortho I	Ortho II	Cubic	Tetragonal
V_0(LDA)	34.98	33.67	29.89	32.89	33.34
V_0(GGA)	36.39	35.04	31.18	34.10	34.82
ΔV_0	1.41	1.37	1.29	1.21	1.48
V_0(GGA)/V_0(LDA)	1.040	1.041	1.043	1.037	1.044
ΔE_0(LDA)	0	5	102	118	95
ΔE_0(GGA)	0	34	282	169	135
ΔE_0(GGA) − ΔE_0(LDA)	0	29	180	51	40

drawn, where s is given by $s = |\nabla n|/2(3\pi^2 n^4)^{1/3}$.[24] Comparing the distributions of pseudoelectron densities for the monoclinic and orthorhombic-I phases, we find that these two phases have similar distributions for a wide range of r_s. However, since the monoclinic phase shows a somewhat broader distribution extending to r_s above 4.0, the distribution of electron densities is more inhomogeneous for the monoclinic phase. For small values of r_s, the distributions are almost independent of the structure, indicating that the localized electron densities around the O atoms are similar to each other. If charge densities are uniformally distributed over the whole space, the distribution of electron densities must be δ function like. As r_s increases above 2.0, we find that the orthorhombic-II phase shows a very different feature, with a large fraction of the Wigner-Seitz cell within the relatively smaller range of r_s. This result indicates that the distribution of electron densities is more homogeneous for the orthorhombic-II phase, compared with the orthorhombic-I phase. This behavior is also confirmed by the distribution of normalized density gradients, with larger volume fractions in the region of small s. The difference in the homogeneity of electron densities between the orthorhombic-I and orthorhombic-II phases is mainly due to the increased coordination numbers of the O and Hf atoms, as discussed earlier. To investigate the correlation between the coordination number and the homogeneity of electron densities, we calculate the electron density distributions within a radius of 2.25 Å around the threefold- and fourfold-

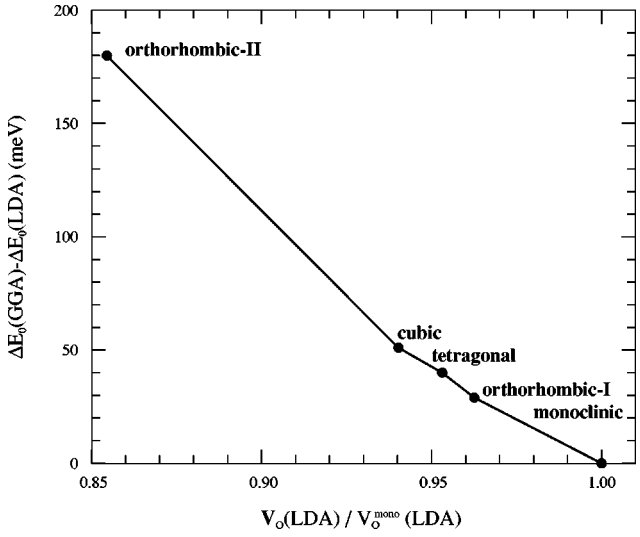

FIG. 7. The increase of the ground-state energy difference with respect to the monoclinic phase, i.e., $\Delta E_0(\mathrm{GGA}) - \Delta E_0(\mathrm{LDA})$, is plotted as a function of the normalized equilibrium volume, $V_0(\mathrm{LDA})/V_0^{mono}(\mathrm{LDA})$.

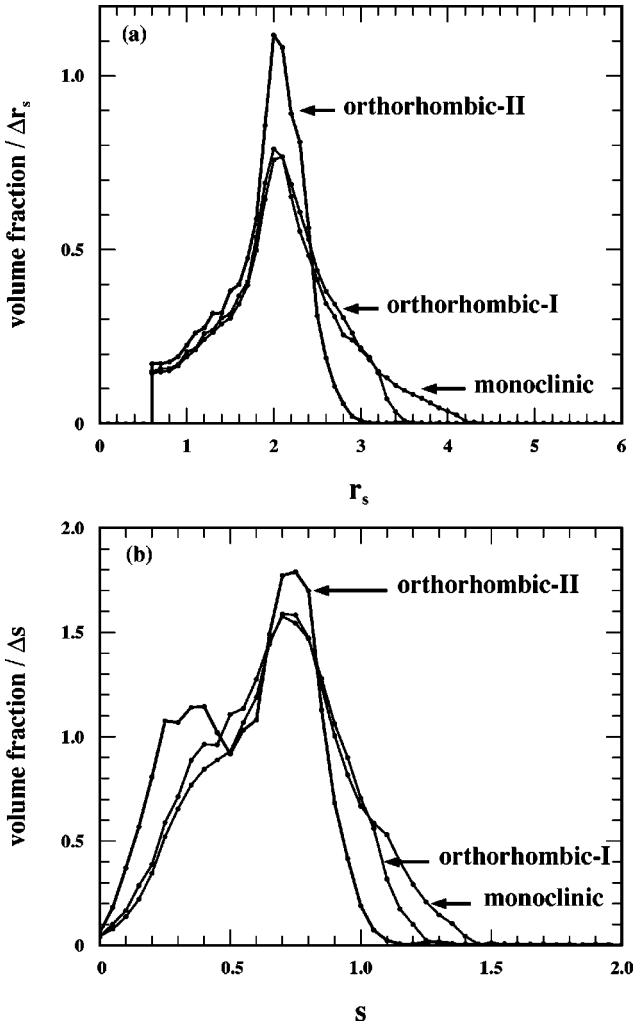

FIG. 8. Distributions of (a) pseudoelectron densities (r_s) and (b) normalized density gradients (s) for the monoclinic, orthorhombic-I, and orthorhombic-II structures in the GGA (see the text for details).

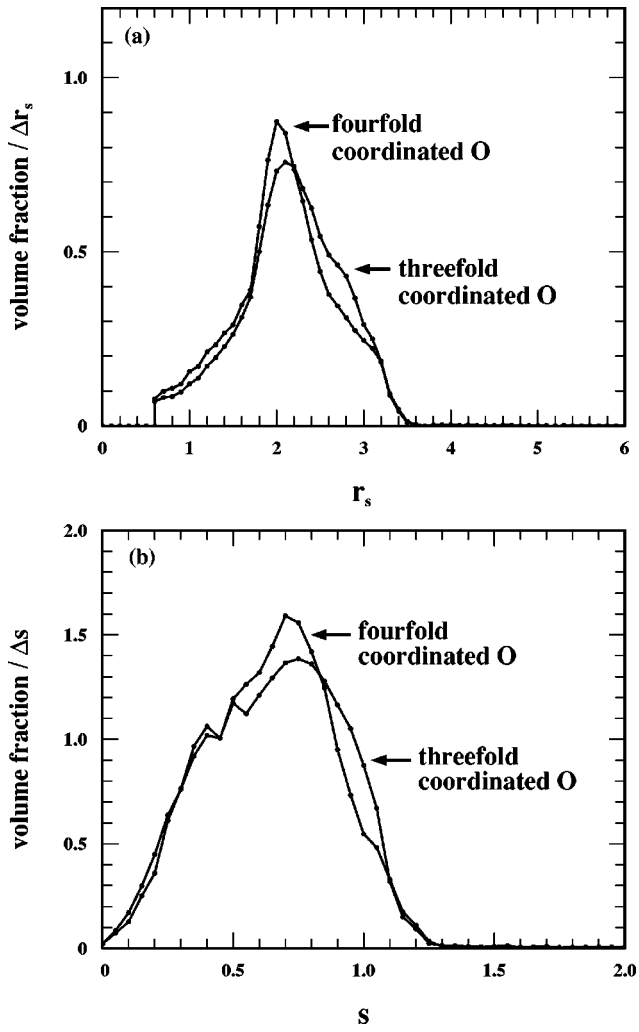

FIG. 9. Distributions of (a) pseudoelectron densities and (b) normalized density gradients around the threefold- and fourfold-coordinated O atoms for the orthorhombic-I structure in the GGA.

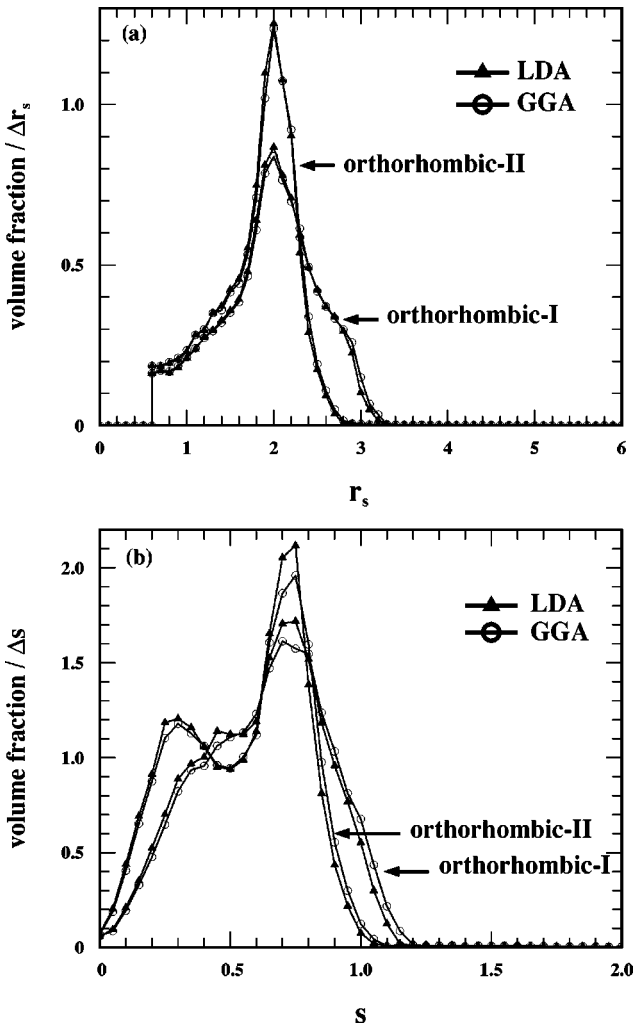

FIG. 10. Distributions of (a) pseudoelectron densities and (b) normalized density gradients for the orthorhombic-I and orthorhombic-II structures within the LDA (solid triangles) and GGA (open circles) calculations.

coordinated O atoms for the orthorhombic-I phase, and find that the volume factions having higher values of s are larger around the threefold-coordinated O atom, as shown in Fig. 9. The inhomogeneity of electron densities is enhanced as the coordination number of the O atom decreases.

It is known that the GGA correction to the total energy increases as the inhomogeneity of electron densities is enhanced. In previous calculations for the diamond–to–β-tin transition of Si,[10] the energy lowering by the GGA was shown to be larger for the more inhomogeneous diamond phase than for the metallic β-tin phase, resulting in a larger energy difference between the two phases and thus increasing the transition pressure. In Fig. 10, we compare the spatial distributions of electron densities which are calculated by the LDA and GGA for the orthorhombic-I and orthorhombic-II phases. For both phases, it is difficult to find any distinct change in the distribution of r_s. However, as compared to the LDA results, the distribution of s clearly shows that the electron densities are more inhomogeneous in the GGA, leading to a larger decrease of total energy. As going from monoclinic to orthorhombic I and to orthorhombic II, the energy lowering becomes less significant because the homogeneity of electron densities increases. In fact, we find that the lowering of the exchange-correlation energy by the GGA correction is larger by about 0.27 eV per HfO_2 for the orthorhombic-I phase than for the orthorhombic-II phase. Thus, as the volume is compressed, the transition pressures are greatly enhanced in the GGA due to the increase of ΔE_0 relative to the monoclinic phase.

IV. CONCLUSIONS

In conclusion, we have investigated the structural phase transition of HfO_2 under pressure through the first-principles pseudopotential calculations. In the GGA calculations, we find that the monoclinic phase transforms to orthorhombic I at 3.8 GPa and then to orthorhombic II at 10.6 GPa. The transition pressures and volume changes are in good agreement with experiments in the GGA, while the LDA severely underestimates the transition pressures. Analyzing the distri-

bution of electron densities, we find that the electron densities of the orthorhombic-II phase are more homogeneous than for the orthorhombic-I phase, mainly due to the increase of the coordination numbers. Thus, the energy difference between the orthorhombic-I and orthorhombic-II phases is greatly increased in the GGA, leading to an increase of the transition pressure.

ACKNOWLEDGMENTS

This work was supported by the third supercomputing application support program of the KISTI and the Ministry of Science and Technology of Korea through the National Science and Technology Program (Grant No. M1-0213-04-0001).

[1] B.H. Lee, L. Kang, R. Nieh, W.-J. Qi, and J.C. Lee, Appl. Phys. Lett. **76**, 1926 (2000).
[2] M. Gutowski, J.E. Jaffe, C.L. Liu, M. Stoker, R.I. Hegde, R.S. Rai, and P.J. Tobin, Appl. Phys. Lett. **80**, 1897 (2002).
[3] O. Ohtaka, H. Fukui, T. Kunisada, T. Fujisawa, K. Funakoshi, W. Utsumi, T. Irifune, K. Kuroda, and T. Kikegawa, J. Am. Ceram. Soc. **84**, 1369 (2001).
[4] A. Jayaraman, S.Y. Wang, S.K. Sharma, and L.C. Ming, Phys. Rev. B **48**, 9205 (1993).
[5] S. Desgreniers and K. Lagarec, Phys. Rev. B **59**, 8467 (1999).
[6] J.M. Leger, A. Atouf, P.E. Tomaszewski, and A.S. Pereira, Phys. Rev. B **48**, 93 (1993).
[7] X. Zhao and D. Vanderbilt, Phys. Rev. B **65**, 233106 (2002).
[8] A.S. Foster, F. Lopez Gejo, A.L. Shluger, and R.M. Nieminen, Phys. Rev. B **65**, 174117 (2002).
[9] J.E. Lowther, J.K. Dewhurst, J.M. Leger, and J. Haines, Phys. Rev. B **60**, 14 485 (1999).
[10] N. Moll, M. Bockstedte, M. Fuchs, E. Pehlke, and M. Scheffler, Phys. Rev. B **52**, 2550 (1995).
[11] D.R. Hamann, Phys. Rev. Lett. **76**, 660 (1996).
[12] N. Troullier and J.L. Martins, Phys. Rev. B **43**, 1993 (1991).
[13] L. Kleinman and D.M. Bylander, Phys. Rev. Lett. **48**, 1425 (1982).
[14] S.G. Louie, S. Froyen, and M.L. Cohen, Phys. Rev. B **26**, 1738 (1982).
[15] D.M. Ceperley and B.J. Alder, Phys. Rev. Lett. **45**, 566 (1980); J.P. Perdew and A. Zunger, Phys. Rev. B **23**, 5048 (1981).
[16] J.P. Perdew, K. Burke, and M. Ernzerhof, Phys. Rev. Lett. **77**, 3865 (1996).
[17] F.D. Murnaghan, Proc. Natl. Acad. Sci. U.S.A. **30**, 244 (1944).
[18] J. Wang, H.P. Li, and R. Stevens, J. Mater. Sci. **27**, 5397 (1992).
[19] D.M. Adams, S. Leonard, D.R. Russel, and R.J. Cernik, J. Phys. Chem. Solids **52**, 1181 (1991).
[20] D.W. Stacy, J.K. Johnstone, and D.R. Wilder, J. Am. Ceram. Soc. **55**, 482 (1972).
[21] D. Vanderbilt, Phys. Rev. B **41**, 7892 (1990).
[22] J.P. Perdew, in *Electronic Structure of Solids*, edited by P. Xiesche and H. Eschrig (Akademie-Verlag, Berlin, 1991).
[23] M. Balog, M. Schieber, M. Michiman, and S. Patai, Thin Solid Films **41**, 247 (1977).
[24] A. Zupan, P. Blaha, K. Schwarz, and J.P. Perdew, Phys. Rev. B **58**, 11 266 (1998).